Proceedings of the ASME 2015 International Design Engineering Technical Conferences & Computers and Information in Engineering Conference
IDETC/CIE 2015
August 2-5, 2015, Boston, Massachusetts, USA

DETC2015-47583

MECHANISM DESIGN AND SIMULATION OF THE ULTRA SPINE, A TENSEGRITY ROBOT

Andrew P. Sabelhaus*
Hao Ji
Patrick Hylton
Yakshu Madaan
ChanWoo Yang
Alice M. Agogino
Department of Mechanical Engineering
University of California Berkeley
Berkeley, California 94705
apsabelhaus, hao.ji, pbhylton, yakshu.madaan, chanwoo.yang, agogino, @berkeley.edu

Jeffrey Friesen
Department of Mechanical Engineering
University of California San Diego
La Jolla, California 92093
Email: jfriesen@ucsd.edu

Vytas SunSpiral
Stinger Ghaffarian Technologies,
Intelligent Robotics Group
Bldg. N269 NASA Ames Research Center
Moffett Field CA 94035
Email: vytas.sunspiral@nasa.gov

ABSTRACT

The Underactuated Lightweight Tensegrity Robotic Assistive Spine (ULTRA Spine) project is an ongoing effort to create a compliant, cable-driven, 3-degree-of-freedom, underactuated tensegrity core for quadruped robots. This work presents simulations and preliminary mechanism designs of that robot. Design goals and the iterative design process for an ULTRA Spine prototype are discussed. Inverse kinematics simulations are used to develop engineering characteristics for the robot, and forward kinematics simulations are used to verify these parameters. Then, multiple novel mechanism designs are presented that address challenges for this structure, in the context of design for prototyping and assembly. These include the spine robot's multiple-gear-ratio actuators, spine link structure, spine link assembly locks, and the multiple-spring cable compliance system.

1 INTRODUCTION

Robots with flexible spines have many potential advantages over those with rigid cores. Generating motion from the robot's core structure could allow for more complex and efficient locomotion for quadrupeds and bipeds, as well as greater ability to traverse unknown terrain and interact with unknown environments while keeping stable and safe. However, spine or flexible-core robots suffer from the tradeoff between compliance, versatility, and amount of actuation (which relates directly to robot mass.) The one-actuator-per-cable model quickly becomes inefficient with an increasing number of cables. The Underactuated Lightweight Tensegrity Robotic Assistive Spine (ULTRA Spine) seeks to create a robot spine that provides compliance in all degrees of freedom as well as versatility in use, while keeping the number of actuators as low as possible. The concepts of tensegrity ("tensile-integrity") systems provide a convenient framework for structured compliance and underactuation, due to the properties of the structure's tension network. This robot design implements such a tensegrity structure, using tetrahedra as the spine links, each link separated without physical contact or joint-induced moment arms.

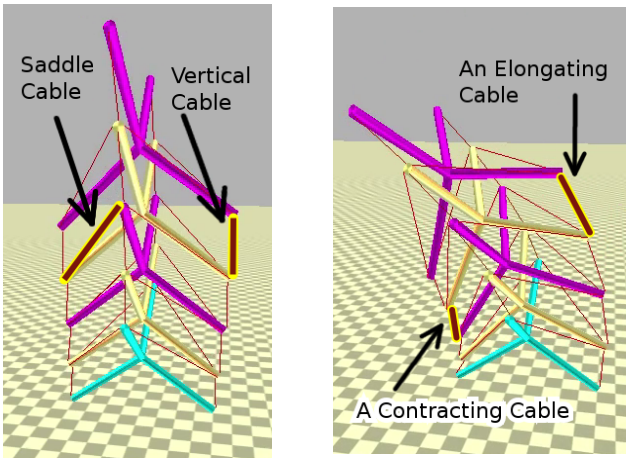

(a) Upright spine in equilibrium, unactuated.

(b) Spine in lateral bending, with actuation.

FIGURE 1: ULTRA Spine in the NASA Tensegrity Robotics Toolkit (NTRT) simulator, under gravitational loading [1].

*Address all correspondence to this author.

Drawing from the designs of many past flexible robots, such as snakes and bio-inspired animal appendages, this design work emphasizes new capabilities such as weight-efficient designs and compliance in all degrees of freedom that arise from underactuation. This spine robot also has ability to create complex 3-dimensional kinematics in translational, axial, and torsional directions with a minimum number of actuators for many cables. After reviewing prior work and placing this robot in context, the design process is discussed for this spine. Then, simulations of the kinematics of the robot are used to estimate engineering characteristics such as cable forces. Finally, mechanical designs are presented, based on the simulations, that implement novel solutions to the challenges of a highly underactuated cable-driven system. Future work will include more designs for the torsional actuation system, and physical prototyping of this robot.

2 BACKGROUND AND PRIOR WORK

Much prior work has explored the design and implementation of snake and spine-like robots, both in the context of robot chassis or cores and independent manipulators. One direction of research involves rigid body spine robots, which use mechanical joints or hard-body contact to constrain the robot's movement. Such robots include Salamandra [2–4], the spines by Inaba et al. [5], the elephant trunk robot from the Walker group [6, 7], and the many snake robots from Choset [8–11]. Current full-body robots have begun to implement low-degree-of-freedom spine joints similar to these past robots, including the recent MIT Cheetah design [12, 13]. Though these designs are robust, the stiffness and high forces from the rigid joints can be undesirable when interacting with unknown terrain or sensitive objects.

Others have constructed manipulator robots that are completly soft, such as OctArm from the Walker group [14, 15] and the octopus arm by Laschi et al. [16, 17]. Pneumatics are common, even in prior tensegrity robotics work [18, 19]. However, these robots require significant external equipment, which can be difficult to integrate into a robotic system without a dramatic increase in complexity and weight.

Tensegrity systems have the unique ability to be flexible in all degrees of freedom, lightweight, and independent of large supporting hardware [20, 21]. Ideal tensegrity structures consist of rigid compressive elements (rods) held together in a tension network (cables) such that no two rigid bodies touch [22]. Without rigid contact, ideal systems have no bending moments, and thus compressive elements can be much thinner. Additionally, tensegrity structures passively distribute forces through the tension network, as opposed to concentrating moment arms at mechanical joints. The biological motivation for tensegrity systems also compels these systems' use in robotics [23, 24].

Robot designs using tensegrity structures are a relatively new concept, pioneered by Lipson and Paul et al. [25]. MiratsTur has presented design and controls work on various other tensegrity morphologies that have been tethered or fixed to the ground [26, 27]. At Union College, Rieffel and colleagues are following an interesting line of work by considering vibration based actuation for small tensegrities [28]. Related work was presented by Böhm and Zimmermann, who demonstrated controlled locomotion of vibration driven tensegrity robots with a single actuator [29]. Finally, the authors' work in the Dynamic Tensegrity Robotics Lab at NASA Ames Research Center's Intelligent Robotics Group has been pioneering new morphologies and control strategies for tensegrity robots, including autonomous rolling spheres [1, 30–32], crawling snakes [33, 34], and climbing robots [35].

ULTRA Spine builds upon past work in multiple novel ways, two of which are highlighted here. First, ULTRA Spine is designed towards a performance specification: unlike the robots in [33, 34] which are designed to demonstrate some general class of motion, ULTRA Spine has actuators, mechanisms, and structural elements designed against engineering requirements of specific movements which can thus be compared directly to simulation results. More importantly, ULTRA Spine heavily emphasizes underactuation, and introduces new designs for parallel underactuation in cable-driven systems. In this work, the term *underactuation* is used in two meanings. As with most tensegrities, the system model of ULTRA Spine has fewer possible control inputs than system states, and is thus underactuated [36]. However, in the context of a cable-driven system, ULTRA Spine is also *underactuated* in that multiple cables are controlled by one of its actuators in parallel, as opposed to other tensegrity robots which attach independent actuators to each cable [1,30–35]. This creates the unique challenge of fixing each cable's length change with respect to the others controlled by the same actuator, addressed in simulation in section 4 and in hardware in sections 5.2 and 5.4.

3 DESIGN PROCEDURE AND OBJECTIVES

ULTRA Spine was designed using a combination of simulation iterations and a-priori knowledge about structure morphology and parameters, allowing for focus on the novel underactuated properties of the robot. The design for the first prototype is a filtered result of evaluation and testing through forward and inverse kinematics simulations, selection of discrete mechanical components such as motors and springs, all within the context of rapid prototyping constraints. Component selection was driven by mathematical results and simulations output for gear ratios, forces, masses, and geometric constraints. The feasible options were evaluated in terms of design for manufacturing and assembly. A key component of this design phase was to keep the mechanism simple and easy to modify so as to easily debug any failures.

3.1 Tensegrity Spine Morphology

There are several existing tensegrity structures which have a form resembling a spinal column. Motivations regarding topology selection included minimizing cable count while still maintaining a broad configuration space of this robot in its actuated 3-degrees-of-freedom. These actuation modes were inspired by the motions that are commonly seen in vertebrate animals: bending in two dimensions and torsion around the primary spine axis.

The Flemons spine model [37] exhibited many of these desirable traits. This design consists of stacked tetrahedrons (called *links* in this work) connected to each other by four columns of vertical cables and four *saddle cables*, and can be seen in simulation in Figure 1 as per section 4.2. The topology has a smooth and continuous set of statically stable configurations throughout the bending and torsional motions desired. We will also show below that certain subsets of cables within the structure lend themselves to linked actuation because their length changes can be shown to be linearly related during the desired bending motions.

All models of ULTRA Spine below assume that the cables in the model are each connected to a spring, but no damper.

3.2 Iterative Design Procedure

Since there was no clear design goal relating to the size or weight of this spine, simulations were used in combination with system component selection to converge upon a prototype geometry. Starting from the geometry of prior work on similar tetrahedral tensegrity structures [33–35], inverse and forward kinematics simulations were used to estimate forces and cable lengths given robot geometry and weight, which were then iteratively updated based upon the selection of physical components which were rated for such engineering characteristics. These simulations are described in section 4.

One important note about this work is the emphasis on certain subsets of underactuated cable designs. As explained later, only the vertical cables are modeled in both hardware and software for proof-of-concept underactuation: the saddle cables are left for future work.

Figure 1 highlights the saddle cables and elongating/contracting cables in ULTRA Spine, as termed in this section.

4 KINEMATICS AND FORCE SIMULATIONS

Two types of simulations were performed to generate and check the engineering characteristics for the prototype geometry of this spine robot. First, an inverse kinematics script[1] was used to generate cable forces and length changes, then those estimated length change ratios (gear ratios for underactuation) were forward-simulated using the NASA Tensegrity Robotics Toolkit (NTRT) [1].

[1] https://github.com/apsabelhaus/TensegritySpineInverseKinematics

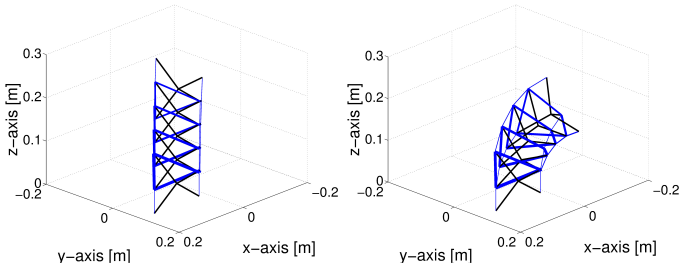

(a) Upright/Straight (b) Bent

FIGURE 2: Inverse Kinematics Simulation Example

4.1 Inverse Kinematics and Forces

The first technique used to determine cable tensions and length changes within the spine was the force density method applied to the problem of inverse kinematics, resulting in the bending motion plots shown in Figure 2. Given the desired nodal positions of the tensegrity structure as well as all nodal forces the structure is subjected to, this algorithm is used to determine a possible set of force densities to allow static equilibrium. The forces on nodes here are caused by gravity, which distribute to the forces in the tension network. The method used was presented in previous work on a similar topology tensegrity robot [35].

The force density method uses a connectivity matrix which serves as a coordinate transform between the local and external frames allowing the problem to be formulated in a linear frame. For a tensegrity with r bars, s cables, and n nodes, the topology will have a connectivity matrix, $\boldsymbol{C}(\in \mathbb{R}^{(s+r)\times n})$, where the first s rows of $\boldsymbol{C}$ correspond to cable members and the last r rows of $\boldsymbol{C}$ correspond to bar members. If member k connects nodes i and j $(i < j)$ then the ith and jth elements of the kth row of $\boldsymbol{C}$ are set to 1 and -1, respectively, as

$$\boldsymbol{C}_{(k,l)} = \begin{cases} 1 & \text{if } l = i, \\ -1 & \text{if } l = j, \\ 0 & \text{otherwise.} \end{cases} \tag{1}$$

Let $\boldsymbol{u}$ be used as a place holder for $\boldsymbol{x}$, $\boldsymbol{y}$, and $\boldsymbol{z}$ $(\in \mathbb{R}^n)$ which will denote the nodal coordinate vectors in the x, y and z directions, respectively. Since cable forces are only applied at nodes in a class-2 tensegrity system like ULTRA Spine [22], the equations for static equilibrium can be expressed as

$$\boldsymbol{C}^T \boldsymbol{Q}\boldsymbol{C}\boldsymbol{u} = \boldsymbol{p}_u, \tag{2}$$

where $\boldsymbol{p}_u$ are the vectors of external loads applied to the nodes in the x, y and z directions, respectively, $(\cdot)^T$ denotes a matrix

transpose, and $\boldsymbol{Q}(\in \mathbb{R}^{(s+r)\times(s+r)})$ is the diagonal square matrix described as $\boldsymbol{Q} = diag(\boldsymbol{q})$ such that $\boldsymbol{q}$ is the force density vector, described as, $\boldsymbol{q} = \{q_1, q_2, q_3, ...q_{s+r}\}^T$, where each entry q_i is defined as the ratio between the force, f_i, and the length, l_i, such that $q_i = f_i/l_i$ is the force density in the member. Substituting $\boldsymbol{Q}$ into (2) yields

$$\boldsymbol{C}^T diag(\boldsymbol{q})\boldsymbol{C}\boldsymbol{u} = \boldsymbol{p}_u, \tag{3}$$

Equation (5) can then be reordered as

$$\boldsymbol{C}^T diag(\boldsymbol{C}\boldsymbol{u})\boldsymbol{q} = \boldsymbol{p}_u, \tag{4}$$

We can then substitute x, y and z back in for u and arrange as,

$$\boldsymbol{A} = \begin{bmatrix} \boldsymbol{C}^T diag(\boldsymbol{C}\boldsymbol{x}) \\ \boldsymbol{C}^T diag(\boldsymbol{C}\boldsymbol{y}) \\ \boldsymbol{C}^T diag(\boldsymbol{C}\boldsymbol{z}) \end{bmatrix}, \tag{5}$$

and

$$\boldsymbol{p} = \begin{bmatrix} \boldsymbol{p}_x \\ \boldsymbol{p}_y \\ \boldsymbol{p}_z \end{bmatrix}, \tag{6}$$

Which allows the problem to be written as a simple linear system of equations,

$$\boldsymbol{A}\boldsymbol{q} = \boldsymbol{p}. \tag{7}$$

Equation (7) can be solved using the Moore-Penrose Pseudoinverse, with the general solution expressed as

$$\begin{bmatrix} \boldsymbol{q}_s \\ \boldsymbol{q}_r \end{bmatrix} = \begin{bmatrix} (\boldsymbol{A}^+)_s \\ (\boldsymbol{A}^+)_r \end{bmatrix} \boldsymbol{p} + \left(\begin{bmatrix} \boldsymbol{I}_s \, 0 \\ 0 \, \boldsymbol{I}_r \end{bmatrix} - \begin{bmatrix} (\boldsymbol{A}^+\boldsymbol{A})_s \\ (\boldsymbol{A}^+\boldsymbol{A})_r \end{bmatrix} \right) \boldsymbol{w} \tag{8}$$

where the equations have been split between the first s rows and the last r rows to represent which elements contribute to cable force densities and bar force densities. A cost function should be selected which minimizes the required cable force densities for a given pose but that doesn't incorporate bar force densities. Therefore a straightforward choice is the norm of $\boldsymbol{q}_s$. A constraint must also be placed on $\boldsymbol{q}_s$ to enforce positivity to prevent slack cables. The optimization can then be written as,

$$\begin{aligned} \underset{\boldsymbol{w}}{\text{minimize}} \quad & \boldsymbol{w}^T\boldsymbol{V}^T\boldsymbol{V}\boldsymbol{w} + 2\boldsymbol{w}^T\boldsymbol{V}^T(\boldsymbol{A}^+)_s\boldsymbol{p} \\ \text{subject to} \quad & {}^T(\boldsymbol{A}^+)_s\boldsymbol{p} + \boldsymbol{V}\boldsymbol{w} \geq 0, \end{aligned} \tag{9}$$

Here $\boldsymbol{w}$ represents a vector of free variables to be optimized, whose length corresponds to the number of columns in $\boldsymbol{V}$. Previously we selected $\boldsymbol{V}$ to equal $(\boldsymbol{I} - \boldsymbol{A}^+\boldsymbol{A})_s$ or the first s rows of the matrix which represents the nullspace of $\boldsymbol{A}$. This choice will produce the correct solution but since $\boldsymbol{V}$ would be an s by $(s+r)$ matrix, its rank will be less than or equal to s. By instead reducing $\boldsymbol{V}$ to an orthogonal matrix whose columns are a basis of the original matrix, we simultaneously reduce the number of free variables in the optimization and also enforce that $\boldsymbol{V}^T\boldsymbol{V}$ will be positive-definite, ensuring convexity.

A quadratic program was then implemented using an interior point method similar to [38] to solve (9) and determine appropriate values for $\boldsymbol{q}$. Other methods, including particle swarm optimization algorithms, have also been used to find the desired optimal solution from the homogeneous solution set of (8) for parallel cable driven systems [39]. These optimization algorithms are more complex and their advantages, namely the ability to handle undesirable problem features such as local minima, are not needed for our application since this cost function is convex.

Once $\boldsymbol{q}$ is known, it is straightforward to use this information to determine cable tensions, recalling that each cable is attached to a spring. This information can then be used to select appropriate spring constants, motor characteristics and cable properties.

Given the $\boldsymbol{q}$ vector found through simulation, the force on each cable was calculated by multiplying a current cable length to the corresponding element in the $\boldsymbol{q}$ vector. Then, the rest length could be back calculated using the length of the cables at each iteration and their respective spring constants, by

$$\boldsymbol{L}_{0i} = \boldsymbol{L}_{\boldsymbol{i}} - \frac{\boldsymbol{L}_{\boldsymbol{i}} \times \boldsymbol{q}(\boldsymbol{i})}{\boldsymbol{K}} \tag{10}$$

where $\boldsymbol{L_0}$ is the rest length, $\boldsymbol{L}$ is the total length of a cable, $\boldsymbol{K}$ is the spring constant for each cable (common across all cables), and $\boldsymbol{i}$ is the index that indicates the specific cable of the tensegrity structure. Here, $\boldsymbol{i} = \{1, 2, ..., 32\}$ for each of the 32 cable segments in this model of ULTRA Spine with 5 tetrahedra.

The rest lengths of the springs on each vertical cable change as a motor pulls or releases the cable, so with an assumption that the spooled cable is not stretched, the ratios of cable rate-of-retraction could be found by taking the ratios of these cable rest lengths. This gave the gear ratios for the acutator.

The simulation structural model, however, differs from the ULTRA Spine prototype in that the simulation only indirectly

models the underactuation. Vertical cables of the simulation model connect only two adjacent tetrahedral segments, while the vertical cables of the proposed robot design connect multiple segments; the connectivity of the saddle cable is the same. To calculate these ratios for underactuation, the vertical cable lengths are modeled as

$$\begin{aligned} \boldsymbol{L}_{0,1-5} &= \boldsymbol{L}_{0,1-2} + \boldsymbol{L}_{0,2-3} + \boldsymbol{L}_{0,3-4} + \boldsymbol{L}_{0,4-5} \\ \boldsymbol{L}_{0,1-4} &= \boldsymbol{L}_{0,1-2} + \boldsymbol{L}_{0,2-3} + \boldsymbol{L}_{0,3-4} \\ \boldsymbol{L}_{0,1-3} &= \boldsymbol{L}_{0,1-2} + \boldsymbol{L}_{0,2-3} \end{aligned} \tag{11}$$

where subscripts represent the cable connectivity between segments, and the index number starts from the bottom to top tetrahedral segment. Then, the changes in each vertical cable length over the simulation step were computed and plotted. Note that since this work concentrates on vertical cables, the saddle cable data is not provided here.

Several parameters are required to be selected a-priori in order to initialize the inverse kinematics iterative design process. First, the lengths of each edge of the tetrahedron were set to $20cm$. Also, as stated above, the applied forces here are those due to gravity, assumed to act at the centroid of each tetrahedron. The initial force density (for the optimization) was selected to be $200N/m$ from prior simulations. Similarly, the spring constant was set to $1220N/m$ for all cables, and the mass of each single tetrahedron segment was specified to be $1.6kg$ (a safety factor of 2 above the current design's projected mass of $0.8kg$.) The bending angle between adjacent spine links was varied from 0 to $0.2rad$, based on a qualitative examination of the bounds of the robot's configuration space. These values will be used for the remainder of the simulation discussion.

Cable Connectivity	Segment 1-2	Segment 1-3	Segment 1-4	Segment 1-5
Initial Rest Length [m]	0.04748	0.09497	0.14250	0.23910
Final Rest Length [m]	0.05978	0.11960	0.17940	0.18990
$\Delta Length$ [m]	0.01230	0.02463	0.03690	0.04920
Gear Ratio	$\times$ 1.00	$\times$ 2.00	$\times$ 3.00	$\times$ 4.00

TABLE 1: Gear Ratio Computation with Elongating Vertical Cable Length Change

The positions of successive tetrahedron for the inverse kinematics calculations were generated by rotating each rigid body's coordinates away from the primary axis by small angles. Each rotation introduced a step change in tetrahedron angle (and thus position, through bending) up to the $0.2rad$ max.

These simulations showed that the length changes for each cable are linear, and results are thus summarized in Tables 1 and 2 instead of plots. Gear ratios for the multiple vertical cables are calculated by dividing the change in the shortest cable length and the change in each of the other 4 cable lengths, as per (11).

The computed gear ratios for the contracting versus elongating vertical cables were slightly different. Mechanism design considerations suggested that the gear ratio by the stretching cable in Table 1 is more appropriate to use in hardware. If the gear ratio of the contracting cables, which is larger than the gear ratio by stretching cable, is used, then the stretching cable would experience much higher tension forces due to larger pulling by a motor and this would induce larger stresses on the hardware. Also, using the smaller gear ratio on the contracting cable would still induce bending, but no extra stress is exerted on the tetrahedrons.

Cable Connectivity	Segment 1-2	Segment 1-3	Segment 1-4	Segment 1-5
Initial Rest Length [m]	0.04610	0.09219	0.13820	0.18410
Final Rest Length [m]	0.03056	0.06059	0.08745	0.11170
$\Delta Length$ [m]	0.01554	0.03160	0.05075	0.07240
Gear Ratio	$\times$ 1.00	$\times$ 2.03	$\times$ 3.26	$\times$ 4.66

TABLE 2: Gear Ratio Computation with Contracting Vertical Cable Length Change

In addition to the cable lengths, tension forces exerted on each cable were computed. Again, computing the cable force on vertical cables also had to consider the structural difference between the simulation model and the proposed prototype model. It was assumed that the pretensions on all vertical cables at the upright state are the same. The simulated tension force on vertical cables were subtracted by this pretension force, and then tensions are added to successive cables to calculate the estimated force on each. This can be represented in equations as

$$\begin{aligned} \boldsymbol{F}_{1-5}(\boldsymbol{\theta}) &= \boldsymbol{F}_{1-2}(\boldsymbol{\theta}) + [\boldsymbol{F}_{2-3}(\boldsymbol{\theta}) - \boldsymbol{F}_{2-3}(\theta_0)] \\ &+ [\boldsymbol{F}_{3-4}(\boldsymbol{\theta}) - \boldsymbol{F}_{3-4}(\theta_0)] + [\boldsymbol{F}_{4-5}(\boldsymbol{\theta}) - \boldsymbol{F}_{4-5}(\theta_0)] \\ \boldsymbol{F}_{1-4}(\boldsymbol{\theta}) &= \boldsymbol{F}_{1-2}(\boldsymbol{\theta}) + [\boldsymbol{F}_{2-3}(\boldsymbol{\theta}) - \boldsymbol{F}_{2-3}(\theta_0)] \\ &+ [\boldsymbol{F}_{3-4}(\boldsymbol{\theta}) - \boldsymbol{F}_{3-4}(\theta_0)] \\ \boldsymbol{F}_{1-3}(\boldsymbol{\theta}) &= \boldsymbol{F}_{1-2}(\boldsymbol{\theta}) + [\boldsymbol{F}_{2-3}(\boldsymbol{\theta}) - \boldsymbol{F}_{2-3}(\theta_0)] \end{aligned} \tag{12}$$

where $\boldsymbol{F}$ represents the vertical cable force and subscripts represent the cable connectivity between segments, and the index number starts from the bottom to top tetrahedral segment. $\boldsymbol{\theta_0}$ is the initial bending angle given at the beginning of the simulation and $\boldsymbol{\theta}$ represents the discrete bending angle such that $\boldsymbol{\theta} = 0.01, 0.02, ..., 0.2$.

These tension forces on vertical cables were calculated and plotted in Figure 3. The force plot for the other two vertical cables are not included because they were not changed during the simulation run. As a result, the maximum cable force exerted on the cable computed by the inverse kinematics simulation was $44.09N$. This force was used in all designs described below.

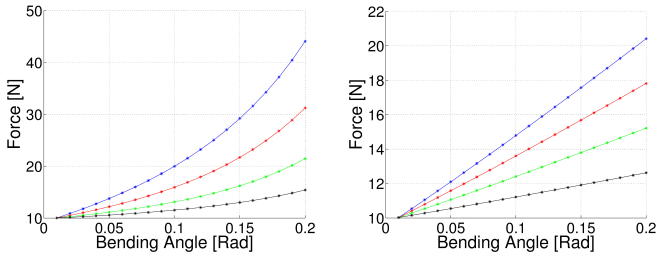

(a) Contracting Vertical Cable (b) Elongating Vertical Cable

FIGURE 3: Vertical Cable Force Changes

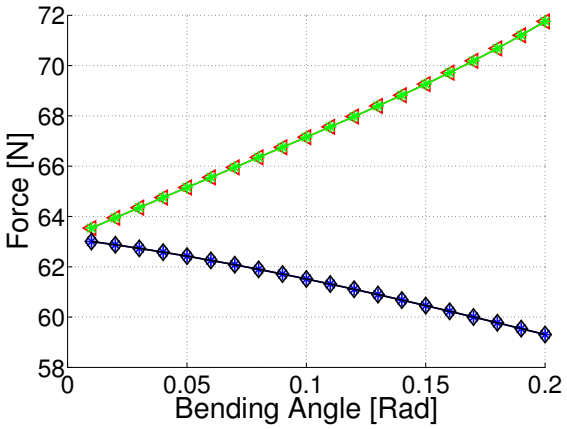

FIGURE 4: Plot of the change in the cable force of the bottom saddle cables, in the inverse kinematics simulation.

Figure 4 shows the change in the cable tension of very bottom saddle cables, between links 1 and 2, which experience the most loading force of tetrahedral segments. This data is included here for thoroughness' sake: though no design work was done for actuating the saddle cables, a rough reality check was desired to ensure that these designs would not fail in the saddle cable subsystem. Blue and black plots represent the saddle cables connected to a node where contracting vertical cables are connected, and red and green plots represent the saddle cables connected to a node where stretching vertical cables are connected. As the tensegrity spine structure bends, it is clear that saddle cables at the contracting side experience larger loading forces, while the other saddle cables at the stretching side experience less forces.

4.2 Forward Kinematics Verification

Once the inverse kinematics script was used to analytically estimate cable lengths and forces for this chosen morphology of the tensegrity spine, a forward kinematics simulation was used to verify that the calculated forces and lengths are reasonable and accurate. Since different gear ratios for elongating and contracting were observed in the inverse kinematics computations (Tables 1 and 2), this simulation was designed to determine if approximations could be made. Specifically, the ULTRA Spine is designed to have only one set of gear ratios for underactuation, so testing was required to ensure that the spine would still function as intended if one set of gear ratios deviate from the ideal calculations above.

The NASA Tensegrity Robotics Toolkit (NTRT) and its simulation environment in C++ (NTRTsim), built on top of the open source Bullet Physics library, is a platform co-developed by the authors [1]. This software, released under the open source Apache2 license, is available online for all researchers[2]. NTRT allows for numerical, physical system simulations with measurements of robot positions and forces. The model of this tensegrity spine morphology created in NTRT is shown in Figure 1, and has the same geometry and mass as the inverse kinematics model created in MATLAB as well as the same set of applied forces (e.g., only those due to gravity.) Prior work discusses the construction and use of NTRT [1].

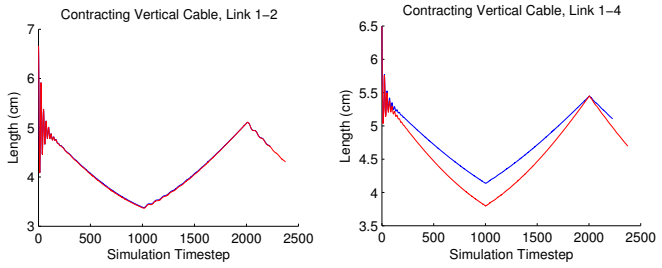

(a) Shortest Cable, Links 1-2 (b) Longest Cable, Links 1-4

FIGURE 5: Forward Kinematics Simulation of ULTRA Spine with Differing Gear Ratios

[2]http://ti.arc.nasa.gov/tech/asr/intelligent-robotics/tensegrity/ntrt/

For this NTRT forward kinematics simulation, the rest lengths of the two vertical cables involved in bending were adjusted slowly (pseudo-kinematically) according to either set of gear ratios, and the total lengths of each cable were recorded. Figure 5 shows these data for two vertical cables in contraction: the shortest contracting cable in 5a and the longest contracting cable in 5b. Blue curves show the cable lengths using the elongation gear ratios (1-2-3-4), and the red curves show these lengths when using the contraction gear ratios (1-2-3.3-4.7).

Multiple observations arise from these results. Importantly, these data show that ULTRA Spine is versatile enough to still generate the desired motion even when ill-tuned. Both Figure 5b and the other simulation data (not shown here) indicate that the robot stays within its configuration space and does not encounter any geometric singularities during this range of bending. The kinematics model of the robot still holds when non-ideal underactuation gear ratios are chosen. And, although the trajectory of the total lengths of the longest cable under the two different gear ratios does not match, its error is small: the most significant length error occurs at 1000 timesteps, with values of

$$\%e = \frac{4.14cm - 3.80cm}{3.80cm} = 8.9\%$$

This percentage of error corresponds to the modeling error in the kinematics that would occur between an ideal mechanical design (using different sets of gear ratios for different vertical cables) versus a practical design, where it is impossible to have different gear ratios for elongating and contracting if the robot is to bend in multiple directions along a given axis. This error is reasonable for prototyping, and could be compensated using an intelligent control system once complex multi-DOF trajectories are desired with vertical cables of the same gear ratios.

5 MECHANICAL DESIGNS

In parallel with these simulations, discrete mechanical components were selected and prototype detail designs were created around them. Specifically, those parameters and components that had the greatest effect on simulation outcomes were chosen first. The following sections describe the primary areas of focus: the core of each tetrahedron link and its attachment with rods, the spring and cable system, and the actuator design with a multi-gear-ratio spindle.

Figure 6 shows ULTRA Spine as a render, with cables connecting its five tetrahedra.

5.1 Spine Link Core and Rod Locking Mechanism

One of the most important goals of the mechanical prototype of this robot is to demonstrate physical motion that validates the forward and inverse kinematic simulations. Consequently, prototyping was emphasized, in the context of ease-of-assembly and ease-of-replacement of parts, such that any deviations from the model could be corrected with minimal effort. The spine link tetrahedron core has mounting locations for both passive and active elements (e.g., the actuator and the internal spring mechanism.) Figure 8 shows one spine tetrahedron link with elements attached. This design provides ease-of-assembly in joining together all four rod-elements of a single tetrahedron.

Additionally, a locking mechanism was designed for attachment of the passive elements to the link core. A small, threaded rod is inserted through the bottom of each passive tube. This smaller threaded rod was kept in place by two custom, circular nuts on the outside of the tubes.. These nuts would then fit into grooves that were cut into the 3-D printed core, and twisted or locked into place. A small machine screw is threaded into the core, securing this lock in place and preventing accidental rod-core separation during operation.

This design facilitates force transfer in shear from the extension springs' hooks to the solid threaded rod and then directly into the tetrahedron core. Alternative designs, which would require drilling or tapping holes into the passive tube, would create stress concentrations and bending moments in the tube. This design allows for a thin-walled tube to be used to constrain the springs, since the tube itself does not experience loads from the spring-connected threaded rod. Figure 7 shows the locking groove on the tetrahedron core, as well as a cross-section view of the locking slot.

Figure 9 shows one of these passive rod assemblies with locking nuts, as explained below.

5.2 Passive Rod Elements and Spring System

A major feature of the underactuated designs on this robot is the presence of both actuated and passive link elements. Each of the cables required compliance in order to fit the simulation models, and this complianece is provided by mechanical springs similar to prior work on tensegrity robots [30,31]. These springs represent the passive rod elements, where cables enter the rod and interact with springs, but are actuated by motors on other links' active elements.

Of the multiple discrete components that required selection at an early design stage, the springs and spring constants for the vertical cables had the closest direct correlation to simulation parameters (through the spring constant K in simulations.) After iterating between simulation and component selection, then adjusting the spring selection as designs of other subsystems progressed, springs with constants of $1220N/m$ were selected. The chosen spring constant is associated with multiple potential off-

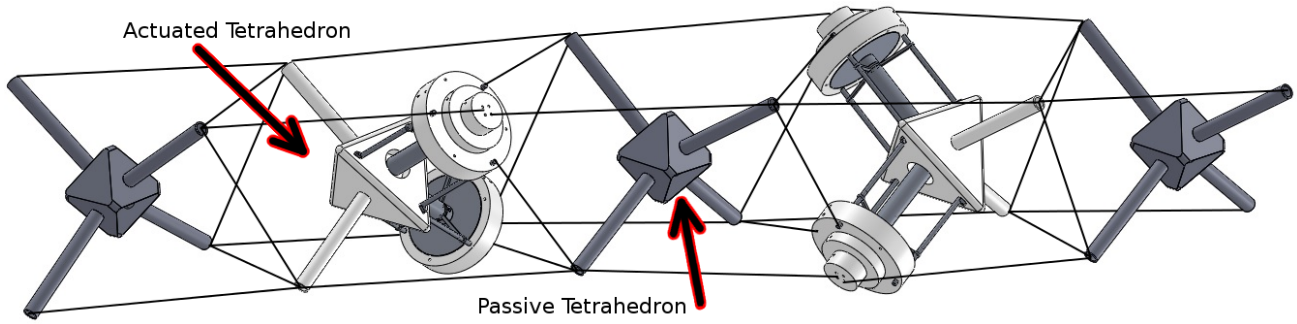

FIGURE 6: Prototype design for ULTRA Spine, rendered as a 3D model, with cable connections.

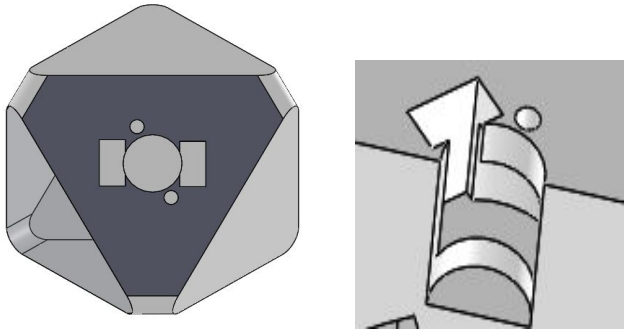

(a) Core with T-Shaped Groove (b) Cross-section of Groove

FIGURE 7: Core with Groove

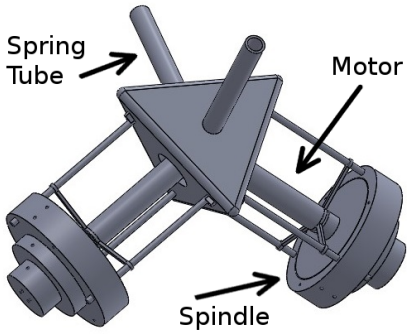

FIGURE 8: Model of one spine tetrahedron, with two actuators and two passive cable tubes connected to one link core.

the-shelf components for a physical spring within the ranges of sizes that were considered reasonable for this robot, allowing for flexibility in detail design. The final component was chosen after the geometry of the spine links was fixed.

For the spring-cable system, multiple qualitative performance goals were associated with the desired ease of prototyping of this robot. Geometrically, two springs must be located inside the same passive link element in order to have each cable be independent. These springs must be constrained to operate in their linear range, so as to avoid permanent deformation and create deviations from the model. Finally, the springs should not experience phenomena such as buckling that would again induce model inconsistencies.

Consequently, a design with extension springs inside plastic tubes was created, such that the tubes can be locked and unlocked from the tetrahedron core, and carry the springs along with them and which to not require disengagement of the cables themselves. Figure 9 shows the multiple constrained spring mechanism, where the only attachment point for the cables is one bar that locks into the core. This design constrains the extension springs with swaged stops on steel cables, keeping the springs from deforming.

In tandem with the motor selection and of possible dimensions for ease of prototyping, the parameters in table 3 were chosen for the springs, spring tubes, threaded rods, and locking mechanism.

Dimensions of Rod Assembly			
Tube Length (in.)	Outer Diameter (in.)	Inner Diameter (in.)	Length of Tube Inside Core (in.)
5.5	0.5	0.375	1
Spring Dimensions			
Outer Diameter (in.)	Extended Length (in.)	Spring Constant (lbs./in.)	Maximum Load (lbs.)
0.25	2.64	6.96	7.03

TABLE 3: Dimensions of Rod Assembly and Springs

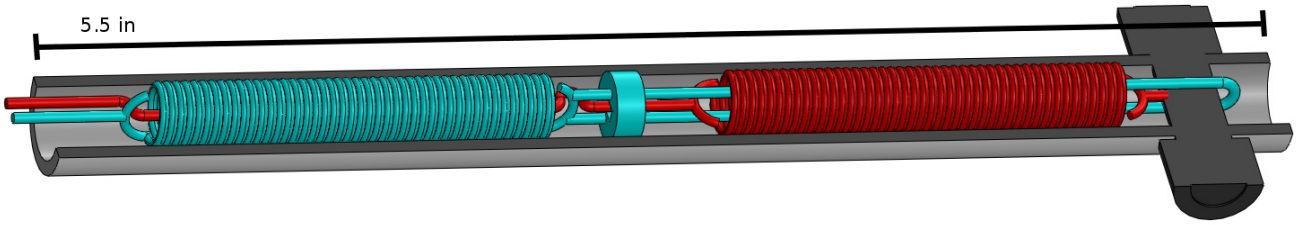

FIGURE 9: Model of the passive spring-cable mechanism, with multiple independent parallel springs axially constrained by swaged nuts on steel cables. The gray Delrin tube and bolt are in cross-section. The red spring and cables are one independent system, as are the blue spring, cables, and constrainig nut. Note that certain features, such as the swaged connections around the threaded bolt and constraining nut, as well as the second constraining nut for the blue spring, are not modeled here.

Evaluation of Cables				
Cable Type	Kevlar	Vectran	Spectra	Dyneema
Strength	+	+	+	+
Creep	+	+	-	+
Splicing	+	+	0	0
Wear	-	+	-	+
Stretch	-	0	0	-

TABLE 4: Comparison of Cables

5.3 Cable Selection

For choosing appropriate cables to connect the individual tetrahedrons and to actuate the robot, multiple materials were evaluated. Since a primary concern for cable-driven robots is lack of cable creep, braided low-deformation plastic cables were the focus of this study. Additional parameters included cable strength, ease of splicing, wear resistance, and frictional properties. Work such as [40] motivates the evaluation of braided cables of Kevlar, Vectran, Spectra, and Dyneema, as do prior tensegrity robots [35].

The diameters considered for these cables were as small as possible from off-the-shelf components, which ranged between approximately 2 mm and 3 mm. The geometric constraints of the springs and tubes also motivated this emphasis on thin cables. The evaluation matrix for this design study is shown in Table 4. These diameters were used in the design of the multi-gear actuator spindle in section 5.4.

The qualitative comparison above implies that the 3 mm Vectran cable is a reasonable choice for this first prototype due to its its low creep, high wear resistance and impressive strength-to-weight properties. More importantly, prior work [32] by the authors has shown that Vectran is easily spliced into reliable cable attachment points.

5.4 Actuator and Gears

Finally, the key crucial component of the ULTRA Spine that allows for underactuation is its multi-gear-ratio actuator. This unit is designed to simulateously adjust the lengths of multiple cables according to the length ratio calculations in section 4.1. As the motors rotate the spindle in Figure 10, cables are wrapped around the device, creating the desired length changes.

Note that this design deviates slightly from the idealized model: the cables exit the spindle at slightly different points, and thus do not align perfectly as in simulation. Since section 4.2 shows that a small amount of error in the model is expected anyway due to the gear ratio difference, such small mechanical sizing inconsistencies are neglected for this prototype.

Geometrically, only four actuators are required for the entire 5-link robot (as in Figure 6), when designed to control two bending modes of ULTRA Spine. These four actuators are oriented orthogonally such that one actuator controls one vertical column of cables, since there are four vertical cable columns.

Motors with maximum torque of $2586mNm$ were selected based on the forces present in the simulation results. It was assumed that the motors will be operated at half current, in order to allow for a safety factor in these designs. ULTRA Spine uses sets of 30W brushless DC motors (Maxon 405813, EC 16mm) reduced by a 157:1 gear box (Maxon 118186). Here, torque output was optimized over speed in order to emphasiz kinematic behavior over dynamic behavior.

This multi-output spindle was designed to locate on the second and the fourth tetrahedral segments, instead of placing all actuators on the bottom link as in the simulations. Unlike the simulations, the actuators are distributed throughout the robot such that no actuated cable must travel more than 3 links. This intentional safety factor over worst-case geometry further encourages the use of one set of gearing ratios over the idealized multiple sets from simulations, since the 1-4 segment (with the most error) is not present.

This allows the use of more compact multi-geared spindles on the actuators. The multi-output spindle was designed to have 2 gears with the same radius and the other 2 gears with doubled

and tripled radii in order to meet this 1-2-3 ratio.

Figure 10 shows the dimensions of the multi-output spindle. The dimensions are determined according to the maximum torque of the motor, the forces on the contractible cables, and the gear ratio. The smallest gear radius was determined by the relationship between the maximum motor torque and the total torque exerted on the multi-output spindle by the vertical cable forces as,

$$\boldsymbol{T}_{max} = \boldsymbol{XF_1} + \boldsymbol{XF_2} + \boldsymbol{2XF_3} + \boldsymbol{3XF_4} \tag{12}$$

where $\boldsymbol{T}_{max}$ is the maximum motor torque, $\boldsymbol{X}$ is the smallest gear radius and $\boldsymbol{F_i}$ represents the tension forces exerted on the contracting vertical cables. Their subscripts represent the forces acting on each cable, and the smallest forces begins with 1, so based on the simulation data, $F_1 = 15.41N$, $F_2 = 21.45N$, $F_3 = 31.24N$, and $F_4 = 44.09N$. The spindle is designed such that the radius of the spindle decreases at greater distances from the motor. By solving the equation for $\boldsymbol{X}$, $\boldsymbol{X} = 11.16mm$, so the minimum diameter of the smallest spindle is 22mm. The other two radii were calculated according to the gear ratios implied in (12).

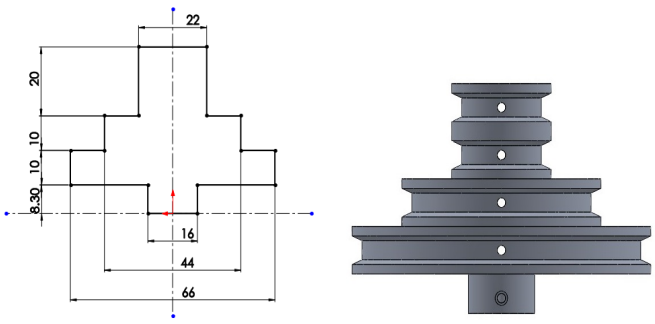

(a) Dimensions of the Multi-output Spindle(mm). (b) CAD of the Multi-output Spindle

FIGURE 10: Multiple-gear-ratio actuator spindle.

6 CONCLUSION AND FUTURE WORK

These simulations and the resulting designs make novel progress toward underactuated motion in tensegrity spines, despite unique challenges. In particular, it was shown that the difference in gear ratios between cables in different directions of motion will cause deviation from an idealized model, resulting in the need for care when designing controllers. However, designs that achieve this underactuation do seem to be possible and within prototyping constraints.

Though the mechanical design phase and some kinematics derivations have been completed, more work is left before this robot is able to show proof-of-concept operation. First, prototyping of the mechanical designs must be completed, and the issues that will inevitably be encountered must be addressed. Cable routing mechanisms must be included for underactuation if friction causes the robot to deviate significantly from the idealized model. Additionally, more analysis must be performed on the saddle cables between tetrahedron links: though these cross-cables can employ the same spring and cable attachment mechanism as the vertical cables, more routing design should occur, as should calibration of the spring constants for those cables. Once the structures have been built, the selected brushless DC motors must be controlled to track force and length trajectories, likely implemented with an impedance control to accurately track both these quantities [33, 34, 41]. Torsional motion, one major advantage of this spine morphology, must be integrated into future iterations of these designs. Finally, force sensors will be included in future designs in order to provide more robust closed-loop control that will not rely on back EMF signals from the motors.

ACKNOWLEDGMENT

This work would not have been possible without the help of the many members of the Berkeley Emergent Space Technologies Lab and the Dynamic Tensegrity Robotics Lab at NASA Ames Research Center's Intelligent Robotics Group. Thanks to Brian Tietz Mirletz, Jonathan Bruce, Ken Caluwaerts, Ryan Adams, Michael Fanton, Paul Glick, Stephen Goodwin, Atil Iscen, Steven Lessard, Kyle Morse, Perry Bhandal and In Won Park from DTRL. Many thanks to BEST lab members including Kyunam Kim, Deaho Moon, Laqshya Taneja, Aliakbar Toghyan, Borna Dehghani, Sarah Dobi, Roya Fallah Firoozi, and Lee-Huang Chen, and Adrian Agogino. Thanks to Terry Fong for his support of tensegrity space robotics at NASA Ames.[3]

Funding for portions of this project was provided under NSF Grant No. DGE 1106400.

[3]The United States Government retains, and by accepting the article for publication, the publisher acknowledges that the United States Government retains, a non-exclusive, paid-up, irrevocable, worldwide license to publish or reproduce the published form of this work, or allow others to do so, for United States Government purposes.

REFERENCES

[1] Caluwaerts, K., Despraz, J., Işçen, A., Sabelhaus, A. P., Bruce, J., Schrauwen, B., and SunSpiral, V., 2014. "Design and control of compliant tensegrity robots through simulation and hardware validation". *Journal of The Royal Society Interface,* ***11***(98).

[2] Ijspeert, A., Crespi, A., Ryczko, D., and Cabelguen, J.-M., 2007. "From swimming to walking with a salamander robot driven by a spinal cord model". *Science,* ***315***(5817), October, pp. 1416–1420.

[3] Crespi, A., and Ijspeert, A. J., 2009. "Salamandra robotica: a biologically inspired amphibious robot that swims and walks". In *Artificial Life Models in Hardware*. Springer, pp. 35–64.

[4] Crespi, A., Karakasiliotis, K., Guignard, A., and Ijspeert, A. J., 2013. "Salamandra Robotica II: An Amphibious Robot to Study Salamander-Like Swimming and Walking Gaits". *IEEE Transactions on Robotics,* ***29***(2), pp. 308–320.

[5] Mizuuchi, I., Inaba, M., and Inoue, H., 2001. "A flexible spine human-form robot-development and control of the posture of the spine". In Intelligent Robots and Systems, 2001. Proceedings. 2001 IEEE/RSJ International Conference on, Vol. 4, IEEE, pp. 2099–2104.

[6] Hannan, M. W., and Walker, I. D., 2001. "Analysis and experiments with an elephant's trunk robot". *Advanced Robotics,* ***15***(8), pp. 847–858.

[7] Hannan, M. W., and Walker, I. D., 2000. "Analysis and initial experiments for a novel elephant's trunk robot". In Intelligent Robots and Systems, 2000.(IROS 2000). Proceedings. 2000 IEEE/RSJ International Conference on, Vol. 1, IEEE, pp. 330–337.

[8] Wolf, A., Brown, H. B., Casciola, R., Costa, A., Schwerin, M., Shamas, E., and Choset, H., 2003. "A mobile hyper redundant mechanism for search and rescue tasks". In Intelligent Robots and Systems, 2003.(IROS 2003). Proceedings. 2003 IEEE/RSJ International Conference on, Vol. 3, IEEE, pp. 2889–2895.

[9] Shammas, E., Wolf, A., Brown Jr, H. B., and Choset, H., 2003. "New joint design for three-dimensional hyper redundant robots". In Intelligent Robots and Systems, 2003.(IROS 2003). Proceedings. 2003 IEEE/RSJ International Conference on, Vol. 4, IEEE, pp. 3594–3599.

[10] Wright, C., Johnson, A., Peck, A., McCord, Z., Naaktgeboren, A., Gianfortoni, P., Gonzalez-Rivero, M., Hatton, R., and Choset, H., 2007. "Design of a modular snake robot". In Intelligent Robots and Systems, 2007. IROS 2007. IEEE/RSJ International Conference on, IEEE, pp. 2609–2614.

[11] Wright, C., Buchan, A., Brown, B., Geist, J., Schwerin, M., Rollinson, D., Tesch, M., and Choset, H., 2012. "Design and architecture of the unified modular snake robot". In Robotics and Automation (ICRA), 2012 IEEE International Conference on, IEEE, pp. 4347–4354.

[12] Folkertsma, G. A., Kim, S., and Stramigioli, S., 2012. "Parallel stiffness in a bounding quadruped with flexible spine". In Intelligent Robots and Systems (IROS), 2012 IEEE/RSJ International Conference on, IEEE, pp. 2210–2215.

[13] Seok, S., Wang, A., Chuah, M. Y., Otten, D., Lang, J., and Kim, S., 2013. "Design principles for highly efficient quadrupeds and implementation on the mit cheetah robot". In Robotics and Automation (ICRA), 2013 IEEE International Conference on, IEEE, pp. 3307–3312.

[14] McMahan, W., Chitrakaran, V., Csencsits, M., Dawson, D., Walker, I. D., Jones, B. A., Pritts, M., Dienno, D., Grissom, M., and Rahn, C. D., 2006. "Field trials and testing of the octarm continuum manipulator". In Robotics and Automation, 2006. ICRA 2006. Proceedings 2006 IEEE International Conference on, IEEE, pp. 2336–2341.

[15] Grissom, M. D., Chitrakaran, V., Dienno, D., Csencits, M., Pritts, M., Jones, B., McMahan, W., Dawson, D., Rahn, C., and Walker, I., 2006. "Design and experimental testing of the octarm soft robot manipulator". In Defense and Security Symposium, International Society for Optics and Photonics, pp. 62301F–62301F.

[16] Laschi, C., Cianchetti, M., Mazzolai, B., Margheri, L., Follador, M., and Dario, P., 2012. "Soft robot arm inspired by the octopus". *Advanced Robotics,* ***26***(7), pp. 709–727.

[17] Mazzolai, B., Margheri, L., Cianchetti, M., Dario, P., and Laschi, C., 2012. "Soft-robotic arm inspired by the octopus: Ii. from artificial requirements to innovative technological solutions". *Bioinspiration & biomimetics,* ***7***(2), p. 025005.

[18] Shibata, M., Saijyo, F., and Hirai, S., 2009. "Crawling by body deformation of tensegrity structure robots". In International Conference on Robotics and Automation (ICRA), pp. 4375 –4380.

[19] Koizumi, Y., Shibata, M., and Hirai, S., 2012. "Rolling tensegrity driven by pneumatic soft actuators". In International Conference on Robotics and Automoation (ICRA), pp. 1988–1993.

[20] Tibert, G., 2002. "Deployable tensegrity structures for space applications". PhD thesis, Royal Institute of Technology.

[21] SunSpiral, V., Gorospe, G., Bruce, J., Iscen, A., Korbel, G., Milam, S., Agogino, A., and Atkinson, D., 2013. "Tensegrity based probes for planetary exploration: Entry, descent and landing (EDL) and surface mobility analysis.". In 10th International Planetary Probe Workshop (IPPW).

[22] Skelton, R. E., and de Oliveira, M. C., 2009. *Tensegrity systems*. Springer.

[23] Ingber, D. E., et al., 1993. "Cellular tensegrity: defining new rules of biological design that govern the cytoskeleton". *Journal of Cell Science,* ***104***, pp. 613–613.

[24] Ingber, D. E., 2003. "Tensegrity i. cell structure and hierarchical systems biology". *Journal of Cell Science,* ***116***(7), pp. 1157–1173.

[25] Paul, C., Valero-Cuevas, F. J., and Lipson, H., 2006. "Design and control of tensegrity robots for locomotion". *IEEE Transactions on Robotics,* ***22***(5), Oct.

[26] Graells Rovira, A., and Mirats-Tur, J. M., 2009. "Control and simulation of a tensegrity-based mobile robot". *Robotics and Autonomous Systems,* ***57***(5), May, pp. 526–535.

[27] Mirats-Tur, J., and Camps, J., 2011. "A three-DoF actuated robot". *Robotics Automation Magazine, IEEE,* ***18***(3), Sept, pp. 96–103.

[28] Khazanov, M., Jocque, J., and Rieffel, J., 2014. "Developing morphological computation in tensegrity robots for controllable actuation". In GECCO, pp. 1049–1052.

[29] Bohm, V., and Zimmermann, K., 2013. "Vibration-driven mobile robots based on single actuated tensegrity structures". In International Conference on Robotics and Automation (ICRA), pp. 5475–5480.

[30] Bruce, J., Caluwaerts, K., Iscen, A., Sabelhaus, A. P., and SunSpiral, V., 2014. "Design and evolution of a modular tensegrity robot platform". In International Conference on Robotics and Automation (ICRA), pp. 3483–3489.

[31] Sabelhaus, A. P., Bruce, J., Caluwaerts, K., Chen, Y., Lu, D., Liu, Y., Agogino, A. K., SunSpiral, V., and Agogino, A. M., 2014. "Hardware design and testing of SUPERball, a modular tensegrity robot". In The 6th World Conference of the International Association for Structural Control and Monitoring (6WCSCM).

[32] Sabelhaus, A. P., Bruce, J., Caluwaerts, K., Manovi, P., Fallah Firoozi, R., Dobi, S., Agogino, A., and SunSpiral, V., 2015. "System design and locomotion of SUPERball, an autonomous tensegrity robot". In Submitted to International Conference on Robotics and Automation (ICRA), Under Review.

[33] Tietz, B. R., Carnahan, R. W., Bachmann, R. J., Quinn, R. D., and SunSpiral, V., 2013. "Tetraspine: Robust terrain handling on a tensegrity robot using central pattern generators". In IEEE/ASME International Conference on Advanced Intelligent Mechatronics (AIM), pp. 261–267.

[34] Mirletz, B., Park, I.-W., Flemons, T. E., Agogino, A. K., Quinn, R. D., and SunSpiral, V., 2014. "Design and control of modular spine-like tensegrity structures". In The 6th World Conference of the International Association for Structural Control and Monitoring (6WCSCM).

[35] Friesen, J., Pogue, A., Bewley, T., de Oliveira, M., Skelton, R., and SunSpiral, V., 2014. "DuCTT: A tensegrity robot for exploring duct systems". In ICRA, pp. 4222–4228.

[36] Reyhanoglu, M., van der Schaft, A., McClamroch, N. H., and Kolmanovsky, I., 1999. "Dynamics and control of a class of underactuated mechanical systems". *Automatic Control, IEEE Transactions on,* ***44***(9), pp. 1663–1671.

[37] Flemons, T., 2012. "The bones of tensegrity". *http://www.intensiondesigns.com/bones_of_tensegrity*.

[38] Loloei, A. Z., Aref, M. M., and Taghirad, H. D., 2009. "Wrench feasible workspace analysis of cable-driven parallel manipulators using lmi approach". In Advanced Intelligent Mechatronics, 2009. AIM 2009. IEEE/ASME International Conference on, IEEE, pp. 1034–1039.

[39] Saber, O., and Zohoor, H., 2013. "Workspace analysis of a cable-suspended robot with active/passive cables". In ASME 2013 International Design Engineering Technical Conferences and Computers and Information in Engineering Conference, American Society of Mechanical Engineers, pp. V06AT07A071–V06AT07A071.

[40] Moyer, T., Tusting, P., and Harmston, C., 2000. "Comparative testing of high strength cord". In 2000 International Technical Rescue Symposium, pp. 1–8.

[41] Orki, O., Ayali, A., Shai, O., and Ben-Hanan, U., 2012. "Modeling of caterpillar crawl using novel tensegrity structures". *Bioinspiration & Biomimetics,* ***7***(4), p. 046006.